Article

Theoretical Study of the Reactive Mechanisms of Li-Doped Ni-Based Oxygen Carrier during Chemical Looping Combustion

Mengke Wang, Minjun Wang,* Ming Xia, Bixiao Zhang, and Yidan Wei

Cite This: *ACS Omega* 2024, 9, 1714−1722

Read Online

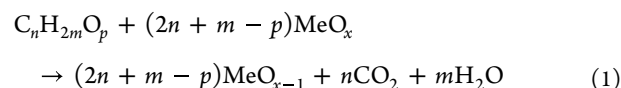ACCESS | 📊 Metrics & More | 📖 Article Recommendations

ABSTRACT: Ni-based oxygen carriers (OCs) are considered promising materials in the chemical looping combustion (CLC) process. However, the reactivity of Ni-based OCs still offers the potential for further enhancement. In this work, the Li doping method has been employed for the modification of Ni-based OCs. The reactivity and microreaction mechanisms of different concentrations of Li-doped Ni-based OCs with CO in CLC are clarified using density functional theory (DFT) simulation. The structures, energy, and density of states are obtained through computational investigation of the reaction path in elementary reactions. The results show that (1) the adsorption energies of CO molecules on NiO surfaces with 4, 8, and 12% Li doping concentrations are −0.53, −0.48, and −0.54 eV, respectively, demonstrating an enhanced reactivity compared to that of pure NiO (−0.41 eV); (2)

the calculation of the transition state indicates that the most favorable pathway for CO oxidation takes place on the surface of NiO with an 8% Li doping concentration, exhibiting the lowest energy barrier of 0.51 eV; and (3) the oxygen vacancy formation energies on the surface of NiO are 3.05, 2.30, and 2.10 eV for 4, 8, and 12% doping concentrations, respectively. Additionally, the decrease in oxygen vacancy formation energies exhibits a gradual decline with an increasing Li doping concentration. By comprehensive analysis, 8% is considered to be the optimal doping concentration of NiO for chemical looping combustion.
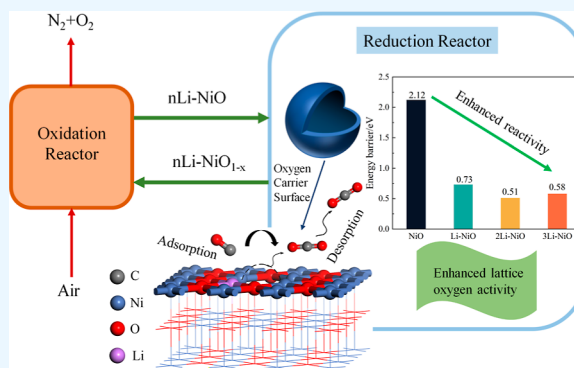
1. INTRODUCTION

Carbon emissions from the usage of fossil fuels are significant sources of greenhouse gases that generate the greenhouse effect.[1,2] The development of efficient capture technologies is imperative for mitigating global CO_2 emissions. The chemical looping combustion (CLC) technology exhibits great potential in achieving complete carbon capture from fuel at a cost-effective rate and with minimal energy penalties.[3,4] The CLC process is illustrated in Figure 1: (i) in the fuel reactor (FR), fuel composition expressed as $C_nH_{2m}O_p$ is oxidized by oxygen carriers (OCs), producing a concentrated stream of CO_2 and H_2O; (ii) the following step involves reoxidizing the decreased

OCs with air in an air reactor (AR). Separation and transport of the oxidized carrier to the fuel reactor before the next cycle follows.[5,6] The simplified reaction equations for the two-step process are listed below. The advantage of CLC lies in the internal separation of CO_2 within the flue gas, resulting in a significant reduction in carbon capture costs.

$$C_nH_{2m}O_p + (2n + m - p)MeO_x$$
$$\rightarrow (2n + m - p)MeO_{x-1} + nCO_2 + mH_2O \quad (1)$$

$$O_2 + 2MeO_{x-1} \rightarrow 2MeO_x \quad (2)$$

The presence of OCs plays a crucial role in facilitating the successful implementation of CLC. To date, over 500 diverse OCs materials suitable for CLC have been investigated, encompassing perovskite-type oxides, natural ores, synthesized materials, and transition metal oxides.[7−13] Transition metal oxides, such as Ni, Co, Fe, Mn, or Cu oxides in various forms,
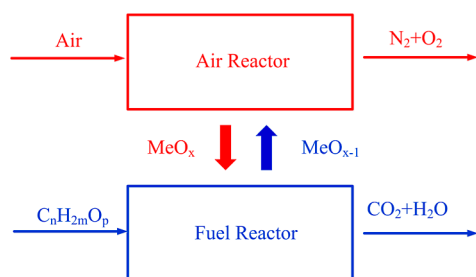

Figure 1. Schematic system of chemical looping combustion.

have been extensively investigated as promising candidates for OCs.[14−17] Among these metal complexes, Ni-based OCs are notable for its exceptional performance at high temperatures (900 to 1100 °C), favorable kinetic properties, and remarkable catalytic proficiency in breaking C−C and C−H bonds.[18−20] However, the utilization of pure NiO in the CLC process is subject to certain limitations, including carbon deposition and lower reaction activity.[21] The efficiency of methane combustion in CLC was observed to decrease with successive cycles due to carbon deposition, as reported by Cheng et al.[22]

The doping technique is widely employed to enhance the reactivity of OCs and exhibits promising prospects for further development.[23−26] Zhang et al.[27] investigated the effects of Fe/Co doping on Ni-based OCs through density functional theory (DFT) calculations and experimental research. The results demonstrated that the doping of Fe enhanced the reactivity of Ni-based OCs, whereas Co doping exerted a detrimental effect on their performance. Yuan et al.[28] studied the reaction mechanism of H_2 oxidation on the surface of Cu-doped Fe-based OCs systematically. The findings suggest that Cu doping enhances the release of lattice oxygen of Fe_2O_3. Wang et al.[24] investigated the influence of Zr doping on the O_2 release of Cu-based OCs using DFT calculations. The results indicate that Zr-doped CuO exhibits enhanced oxygen release compared to pure CuO. Liu and Zachariah[29] synthesized alkali metal (K, Cs, and Na) doped Fe-based oxygen carriers and evaluated the reactivity and stability in a fixed bed reactor for 50 isothermal redox cycles. The findings suggest that the doping of alkali metal can significantly enhance the long-term stability and mitigate carbon deposition.

The incorporation of dopants represents an effective approach for enhancing the chemical stability and reactivity of OCs. Recent research indicates that Li doping as a dopant has potential and benefits in terms of catalyst reactivity. Xu et al.[30] found that using CO oxidation to study the effect on the reactivity and structure of NiO prepared by doping with different Li^+ contents. The results indicate that the intrinsic CO oxidation activity can be remarkably enhanced by adding Li^+ cations. Zhang et al.[31] reported NiO samples doped by Li^+, Zn^{2+} and Cr^{3+} cations were prepared to engineer different amounts of lattice and surface Ni^{3+} cations, and investigated by CO oxidation. It is established that, the intrinsic activity of CO oxidation follows the order of $Ni_{0.9}Li_{0.1}O > NiO > Ni_{0.9}Zn_{0.1}O > Ni_{0.9}Cr_{0.1}O$. Cheng et al.[32] investigated the reactivity performance of Mg−Mn composite OCs enhanced by a low concentration of Li dopant through redox experiments. The results indicate that both Mg_6MnO_8 and $Li−Mg_6MnO_8$ particles consistently exhibit reactivity over 15 redox cycles at 850 °C, demonstrating excellent recyclability. This finding suggests that the limitation of the low melting point of metallic Li does not appear to be evident in Li-doped OCs. In addition, considering the existing literature suggesting that alkali metal doping can mitigate carbon deposition in oxygen carriers, it is plausible to hypothesize that Li doping may also exhibit a similar effect on reducing carbon deposition in Ni-based oxygen carriers. However, this hypothesis necessitates further investigation. Conduct a synthesis of the aforementioned analysis, it is reasonable to speculate that Li doping may have a favorable effect on the performance of Ni-based OCs. However, there are no comprehensive reports on how Li doping affects the performance of Ni-based OCs. Furthermore, studies are scarce on the effects of different Li doping

concentrations on the reactivity and microreaction mechanisms of Ni-based OCs with CO in CLC.

In this work, the reactivity and microreaction mechanisms of different concentrations of Li-doped Ni-based OCs with CO in CLC were investigated by using DFT calculations. The elucidation of the adsorption of CO on the surface of Li-doped Ni-based OCs was achieved. The CO oxidation processes of Li-doped Ni-based OCs were simulated. Additionally, the oxygen vacancy formation energy of Li-doped OCs was calculated. The findings of this study will provide insights into the development of cost-effective and high-performance OCs.

2. COMPUTATIONAL MODEL AND METHODOLOGY

All DFT simulations were conducted in the Cambridge Sequential Total Energy Package (CASTEP)[33] module. The computational method employed in the CASTEP software involves utilizing the DFT plane wave pseudopotential approach. The determination of the total energy was achieved by implementing a self-consistent field (SCF) iteration algorithm. The electron−exchange correlation function was described using the Perdew−Burke−Ernzerh (PBE)[34] generalized function of the Generalized Gradient Approximation (GGA).[35] Ultrasoft pseudopotential[36] was applied to describe ionic cores. The NiO(001) surface has been noted for its higher reactivity in adsorption, making it a preferred choice in prior computational studies focused on CLC.[37−39] Experimental techniques showed that cleavage on (001) planes was easy, resulting in a relatively flat and defect-free surface.[37] Therefore, this particular plane was selected as the reaction surface for investigating NiO in this study.

The utilization of spin-polarized formalism was employed in the NiO unit cell, owing to the antiferromagnetic characteristics of NiO. The DFT + U method was evaluated with U values ranging from 0 to 9 eV, including the specific values of 1, 2.5, 4, 6.3, 8, and 9 eV. It was found that when the U value reaches 6.3 eV, the results exhibited greater consistency when compared to reliable previous calculations data.[40−42] Thus, a U value of 6.3 eV was justified. Consistency exists between the calculated simulated lattice constant of 4.163 Å for bulk NiO and the experimental value of 4.170 Å.[43,44]

A six-layer slab of a (2×2) periodic supercell was adopted to simulate the NiO(001) surface, including both the pure and doped surface. For the doped surface, make the first layer of this surface centered on Ni atoms. The experimental results confirmed that the influence of Li doping on NiO was mainly established by the formation of substitutional solid solutions.[30] In this work, Li doping was achieved by the process of substitutional solid solutions, which involved replacing Ni atoms with Li. A vacuum layer of 15 Å thickness was employed to reduce the interaction between the periodic slabs.[45,46] In the calculations, the top two layers and adsorbate were allowed to relax, while the bottom four layers were kept fixed, as shown in Figure 2. Moreover, multiple substituted Li atoms were taken into consideration. The Ni atoms in the first, second, and third layers of the NiO(001) surface were primarily replaced by Li atoms, labeled as nLi−NiO. The variable "n" represents the number of substituted Li atoms, where n can take values of 1, 2, or 3. In a supercell of 48 atoms, the nLi/Ni ratios correspond to 1/24, 2/24, and 3/24, thus mimicking 4, 8 and 12% Li concentration, respectively. In all calculations, a plane wave cutoff energy of 330 eV was specified. The convergence standards for geometry optimization were set to the maximum
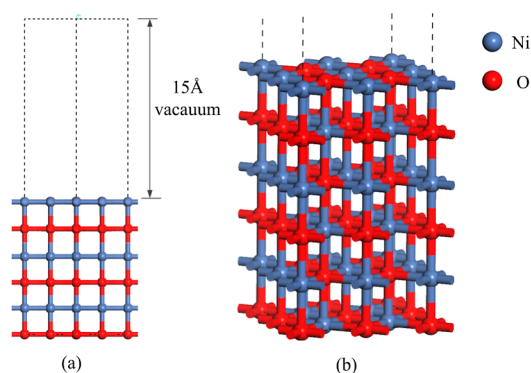
Figure 2. Models of NiO(001) surface: (a) front view and (b) side view.

force, energy, SCF as well as a maximum displacement of 0.05 eV/Å, 2.0×10^{-5} eV/atom, 2.0×10^{-6} eV/atom and 0.002 Å, respectively. The Brillouin zone was used for a $3 \times 3 \times 1$ Monkhorst−Pack k-point grid. The geometry optimization of CO molecules was performed in a $1 \times 1 \times 1$ nm cubic crystal cell to obtain an equilibrium geometry. The bond length of the CO molecule was calculated to be 1.154 Å, which is in considerable accordance with the available theoretical results and experimental values.[47]

To quantify the intensity of the CO adsorbed on the surface of pure and doped, the adsorption energy (E_{ads}) is calculated as follows

$$\Delta E_{ads} = E_{OCs+CO} - (E_{OCs} + E_{CO}) \quad (3)$$

where E_{OCs+CO} is the total energy of the system after adsorption, E_{OCs} and E_{CO} represent the total energy of the clean slab and CO molecule, respectively. Consequently, a more negative E_{ads} usually indicates a stronger adsorption interaction and more stable adsorption configurations.

The LST/QST (linear/quadratic synchronous transit) method determines the transition state (TS) structure, energy barriers, and other information when considering reaction pathways. The energy barrier (E_b) is calculated by the following equation

$$E_b = E_{TS} - E_{IS} \quad (4)$$

where E_{IS} denote the total energy of the initial state (IS), and E_{TS} denote the total energy of the transition state (TS). The higher the energy barriers, the more difficult it is for a reaction to occur and the slower is the reaction rate. The binding energy (E_{bind}) for Li doping is defined as follows

$$E_{bind} = E_{(Li-NiO)} - (E_{NiO} + E_{Ni}) - E_{Li} \quad (5)$$

where $E_{(Li-NiO)}$ is the total energy of the system after Li doping. E_{NiO} is the total energy of the pure NiO supercell. E_{Ni} and E_{Li} are the total energies of the Ni and Li atoms, respectively.

The oxygen vacancy formation energy of OCs can be used to evaluate the surface O activity of OCs. The follows equation is used to calculate the oxygen vacancy formation energy (E_{vac}) of various reactions

$$E_{vac} = E_{def} - E_{per} + 0.5E_{(O_2)} \quad (6)$$

where E_{per} and E_{def} denote the energies of the NiO supercell and the same supercell with one oxygen vacancy, respectively. E_{O_2} is the energy of the O_2 molecule after geometry optimization. With this equation, a smaller E_{vac} value typically indicates a more favorable oxidizing capability of the surface.

3. RESULTS AND DISCUSSION

3.1. Surface Structures of Li-Doped NiO. The surface structures of Li-doped NiO were simulated to investigate the impact of the Li dopants at different concentrations. The optimized configurations for pure and Li-doped NiO are shown in Figure 3. The effect of Li doping on the surface bonding of the O atoms was considered. The binding energy of Li doped saline was calculated to analyze the ease of Li doping at the atomic sites on the NiO surface. The average bond lengths (L_{O-M}) of the dopant sites with adjacent O atoms as well as the binding energies of Li doping on the NiO surface are presented in Table 1. The L_{O-M} bond lengths of the NiO,

Table 1. Corresponding Binding Energy of Li-Doped Surfaces, and the Average Bond Length between the M Atom and Its Near O Atom (M for Ni or Li)

model	E_{bind}/eV	L_{O-M}/Å
NiO		2.085
Li−NiO	−1.67	2.146
2Li−NiO	−1.87	2.245
3Li−NiO	−2.57	2.233

Li−NiO, 2Li−NiO and 3Li−NiO are measured to be 2.085, 2.146, 2.245, and 2.233 Å, respectively. The L_{O-M} bond lengths on NiO surfaces with Li as a dopant are elongated compared to those on undoped surfaces. The results indicate that surface oxygen atoms are activated to some extent following Li doping. The binding energies of the Li−NiO,
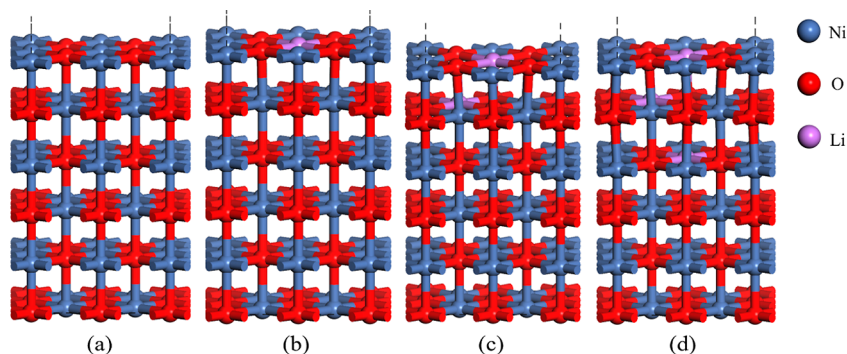

Figure 3. Optimized configurations of (a) pure NiO, (b) Li−NiO, (c) 2Li−NiO, and (d) 3Li−NiO.

2Li−NiO and 3Li−NiO are −1.67, −1.87 and −2.57 eV, respectively. Additionally, all three of these processes are exothermic reactions. The results show that more heat is released as the Li concentration increases.

To investigate the influence of different Li doping concentrations on the model structure of NiO(001), X-ray diffraction (XRD) analysis was performed on the pure and doped OCs. The XRD patterns are listed in Figure 4. The
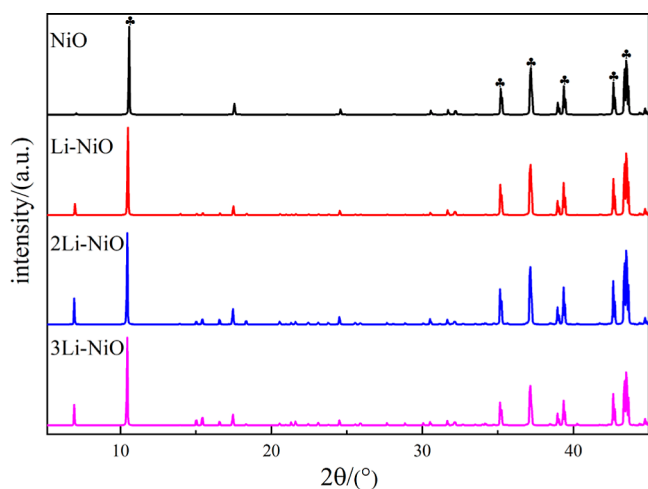

Figure 4. XRD spectra of pure and Li-doped OCs.

experimental data for NiO reveals two prominent peaks at 2θ values of 37.30 and 43.32°.[48] The simulation findings exhibit general agreement with the XRD spectra obtained from the experimental data, with the most prominent peaks observed at 37.15 and 43.40°.[48] Additionally, the incidental peaks between 2θ values of 25 and 45° in the study correspond to those observed in the actual experimental data.[49] This concordance underscores the high accuracy of the computational method employed in describing the crystal structure of the material. The XRD patterns of the Li-doped NiO exhibited minimal deviations from the pure NiO. However, a slight blueshift was observed in the diffraction peaks. Bragg's rule[50] denotes an expansion of the NiO supercell, which may result from the substitution of dopant Li$^+$ ions for Ni^{2+} ions. It is measured that the L_{O-M} bond lengths on NiO surfaces employing Li atoms as a dopant are longer than those on undoped surfaces. Furthermore, the changes in bond length induced by doping correspond to those estimated through XRD analysis. Consequently, these results suggest that varying Li doping concentrations exert minimal influence on the crystal structure of NiO, thereby confirming the applicability of the doping model.

To further comprehend the impact of elemental doping on the structure of OCs, the density of states (DOS) of pure and doped OCs were computed. Figure 5 shows the total DOS for pure and Li-doped NiO. It is observed that the overall alteration in the electronic structure of the NiO bulk phase is negligible following Li doping. The result indicates that despite the influence of different concentrations of Li doping on the local geometry within the system, the overall stability of the OCs remains intact.

3.2. Adsorption of CO on the Surface of NiO. The adsorption of CO at different sites on the surface of pure and Li-doped NiO was investigated. Various adsorption configurations of the CO molecules on the surfaces of OCs were
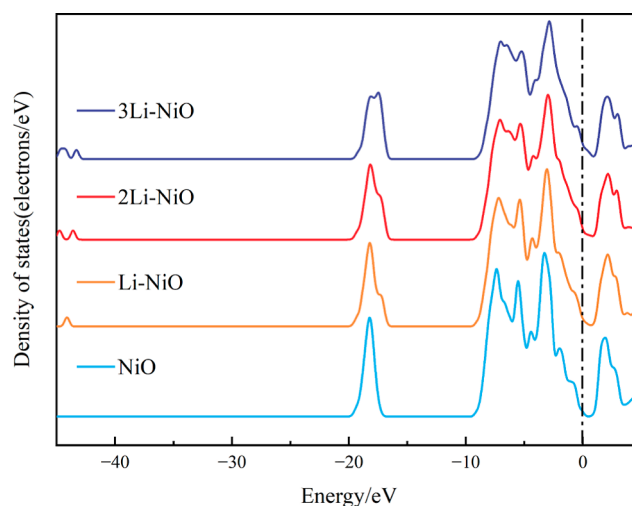

Figure 5. Total DOS for pure and Li-doped OCs.

considered. These configurations included perpendicular adsorption of CO at the Ni top, the O top, and the hollow sites. Moreover, the perpendicular surface adsorption of the CO molecule with C-end and O-end adsorption was considered. Parallel configurations were investigated, where the CO molecule lies flat on the M−O, M···Ni, and O···O bridge sites (denoted as P1, P2, and P3, respectively), where M = Ni or Li. The adsorption configurations are visually represented in Figure 6.
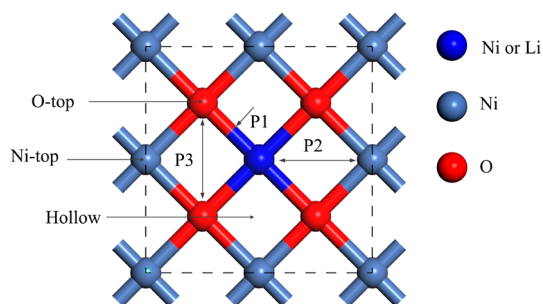

Figure 6. Different CO adsorption sites of pure and Li-doped NiO(0 0 1) surface.

Based on the calculated geometry optimization parameters, the C-terminal perpendicular adsorption of CO at the Ni top site is the most stable configuration on the pure NiO, Li−NiO, and 2Li−NiO surfaces. Additionally, the most stable configuration on the 3Li−NiO surfaces is CO adsorbed at the Ni−O bridge site by the C-end perpendicular adsorption. These most stable configurations of Li-doped NiO surfaces are exhibited in Figure 7. The adsorption energies and structural parameters for each stable configuration are given in Table 2. For the most stable structure, the adsorption energy calculated for the pure NiO surface is −0.41 eV, with the calculated C−Ni distance of 2.051 Å. The calculated C−O bond length of 1.155 Å is approximately equal to the bond length of 1.154 Å for free CO. This result suggests no significant activation of the adsorbed CO. These parameters align with the data obtained from previous calculations, reinforcing the consistency of the findings.[51] The adsorption energies for Li−NiO, 2Li−NiO, and 3Li−NiO are −0.53, −0.48, and −0.54 eV, respectively. It is worth noting that the adsorption energy of the doped surface
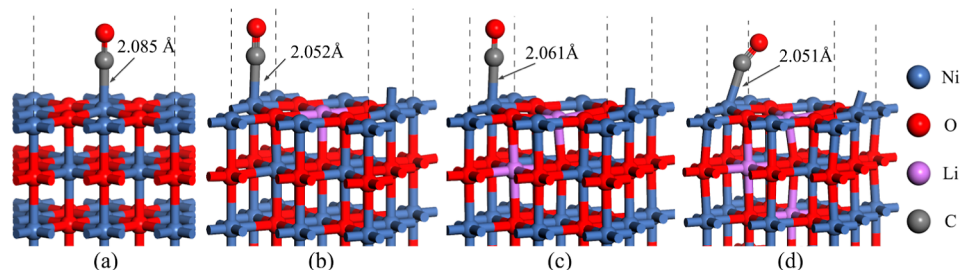
Figure 7. Most stable configurations of CO absorbed on (a) pure NiO(001), (b) Li−NiO(001), (c) 2Li−NiO(001), and (d) 3Li−NiO(001).

Table 2. Adsorption Energy and Structural Parameters for CO after Adsorption on Pure and Li-Doped Surface

model	E_{ads}/eV	Mulliken charge/e	L_{C-O}/Å	L_{C-Ni}/Å
CO		0	1.154	
NiO	−0.41	0.04	1.155	2.085
Li−NiO	−0.53	0.02	1.158	2.052
2Li−NiO	−0.48	0.03	1.156	2.061
3Li−NiO	−0.54	0.01	1.159	2.051

Figure 8. PDOS profiles of the C atom of free CO and adsorbed CO.

with different concentrations of Li atoms is greater than that of the pure surface. Among these configurations, 3Li−NiO is the most exothermic. The results indicate that Li doping promotes the adsorption of CO on the surface. As shown in Table 2, the bond lengths of L_{C-O} are 1.158, 1.156 and 1.159 Å for CO adsorption on Li−NiO, 2Li−NiO and 3Li−NiO surfaces, respectively. The bond lengths of CO to surface Ni atoms are 2.061, 2.052, and 2.085 Å when CO is adsorbed on the Li−NiO, 2Li−NiO, and 3Li−NiO surfaces, respectively. Compared to the pure NiO surface, the adsorbed CO bond length is slightly elongated, and the L_{C-Ni} bond length is shorter, showing that the CO molecule slightly activates the adsorption.

The Mulliken charge distribution of CO was studied to determine the mechanism of bonding between the CO molecules and the surface during the adsorption reaction. The CO charges in NiO, Li−NiO, 2Li−NiO and 3Li−NiO changed from $0e$ prior adsorption to $0.04e$, $0.02e$, $0.03e$ and $0.01e$, respectively. The Mulliken charge population analysis revealed that a limited number of electrons were transported from the CO molecule to the pure and Li-doped NiO surfaces. The charge transfer of CO to Ni-based OCs decreases upon adsorption onto the surface of Li-doped Ni-based OCs compared to that on the surface without Li doping. The decrease in charge transfer is accompanied by an increase in the adsorption energy of CO on the surface of Li-doped Ni-based OCs. Furthermore, the partial density of states (PDOS) of the free CO structures and CO structures following adsorption in the active site were investigated, as shown in Figure 8. The electrical configuration of the CO molecule in its free state is $[(1\sigma)^2(2\sigma)^2(3\sigma)^2(4\sigma)^2(1\pi)^4(5\sigma)^2(2\pi)^0]$. Figure 8 presents the PDOS profiles of the free CO molecule, where the 4σ, 1π, 5σ, and $2\pi^*$orbitals are mostly around −4.95, −2.60, 0.00, and 6.80 eV. The highest occupied molecular orbital (HOMO) of the CO molecule corresponds to the 5σ orbital, located in proximity to the Fermi energy level. Conversely, the lowest unoccupied molecular orbital (LUMO) is attributed to the $2\pi^*$ orbital. Since the 5σ and $2\pi^*$ orbitals of the CO molecule are contributed primarily by the C atom, the C atom is more likely to form a covalent bond with the surface metal. The adsorption mechanism of the CO molecule onto the Ni atom is likely associated with the hybridization process
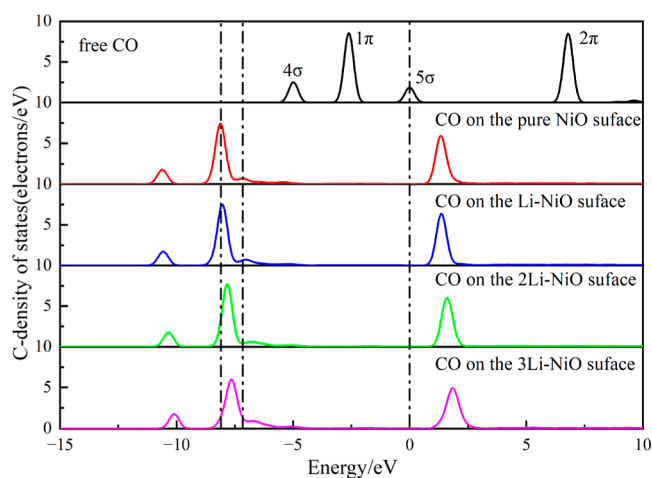
between the 5σ and $2\pi^*$ orbitals of the CO molecule and the 3d orbital of the Ni atom. As depicted in Figure 8, the PDOS of CO following the adsorption reaction demonstrates a left shift in energy compared to the PDOS of free CO molecules. The energy decrease is accompanied by the movement of the 4σ, 1π, 5σ, and $2\pi^*$ orbitals toward lower energy states. These findings demonstrate that the CO molecule can be securely adsorbed on the surface. It is evident from the diagram that there is an overlap between the 1π and 5σ orbitals, leading to the emergence of two new peaks at the overlap. The mutual hybridization of the $2\pi^*$ and 3d orbitals of the C and Ni atoms is responsible for this phenomenon. Moreover, Figure 8 shows slight disparities in the PDOS peaks of CO molecules adsorbed on both the pure and Li-doped NiO surfaces. These suggest that the number of electrons transferred to the various surfaces by the CO molecules varies, a finding consistent with Mulliken charge population analysis.

3.3. CO Oxidation Mechanism of on Pure and Doped NiO Surface. The CO oxidation reaction on the pure and doped NiO surfaces was simulated. The mechanism of CO oxidation on the OCs surface involves three steps: CO adsorption, CO_2 formation, and CO_2 desorption. The oxidation mechanism processes of the most stable structures for NiO, Li−NiO, 2Li−NiO, and 3Li−NiO OCs were considered. Models for the initial state (IS), transition state (TS), intermediate state (IM), and final state (FS) of the oxidation pathway were obtained, as depicted in Figure 9. Afterward, the TS between IS and IM is located. Figure 10 displays the energy profile corresponding to the process. The CO_2 formation energy barrier of pure NiO surface is 2.12 eV. The CO_2 formation energy barriers on the Li−NiO, 2Li−NiO, and 3Li−NiO surfaces are 0.73, 0.51, and 0.58 eV, respectively.
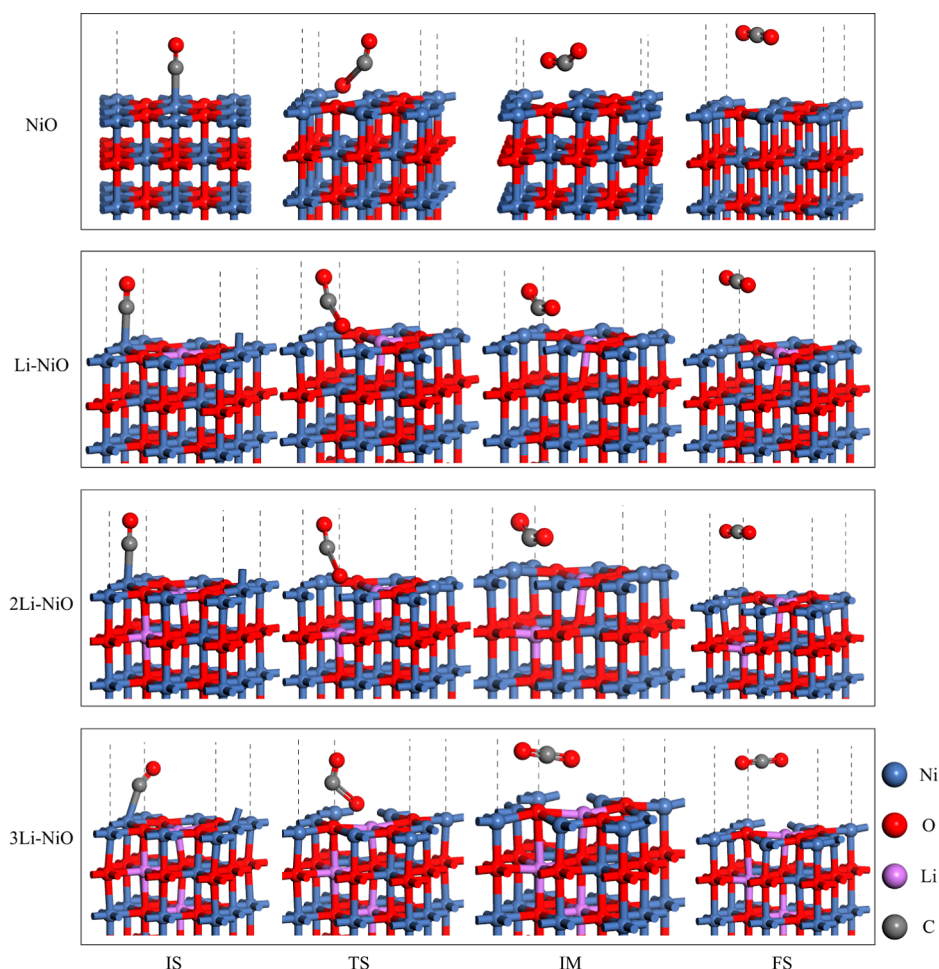
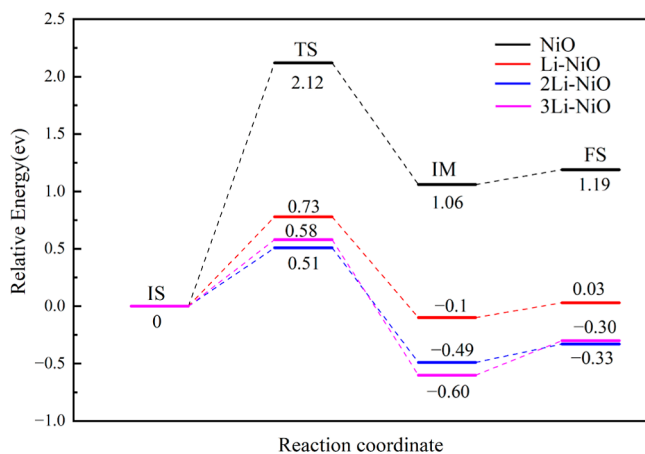**Figure 9.** Reaction pathways for CO oxidation over the NiO surface.

Figure 10. Energy profile of CO in oxidation on the surface of the OCs.

Comparison with the energy barrier on the surface of pure OCs reveals a significant reduction of approximately 1.61 eV on the surface of 2Li−NiO. The varied Li doping doses lower the energy barrier for the CO oxidation process, resulting in a considerable increase in OCs activity. The total process from CO adsorption to CO_2 desorption is endothermic by 1.19 eV. The CO oxidation reaction enthalpies of the Li−NiO, 2Li−NiO, and 3Li−NiO surfaces are 0.03, −0.33, and −0.30 eV, respectively. The CO oxidation on the 2Li−NiO and 3Li−NiO

surfaces is exothermic. Although the entire CO oxidation process on the Li−NiO surfaces is endothermic, the energy barrier and reaction enthalpy are lower than during the pure NiO surface. The above investigations suggest that the addition of Li as a dopant for NiO contributes to enhanced reactivity.

Additionally, the charge distribution between CO and the surface during the CO_2 formation was considered. Figure 11a−d show the electron density profiles of CO at the stable adsorption site. It is observed that the C atom in CO is blue color, while the adjacent O atom appears red, indicating a significant accumulation of electrons around the O atom. The finding suggests the transfer of electrons from the C atom to the O atom. However, there is minimal charge transfer to the surface Ni atom. Figure 11e−h displays the charge density profiles during the oxidation reaction that generates CO_2 on the OCs surface. It finds that an electron cloud overlap exists between the O atoms on the surface of OCs and the C atom. The phenomenon indicates the formation of new covalent bonds between the atom of the OCs surface and the CO molecules, ultimately contributing to the generation of CO_2.

3.4. Oxygen Activity for Li-Doped NiO Surfaces. The primary role of OCs in the CLC process is to provide active lattice oxygen for the surface reactions with fuel molecules. Oxygen vacancies are generated on the surface of OCs when a CO molecule is oxidized. Thus, oxygen vacancy formation energy is often employed to characterize lattice oxygen activity
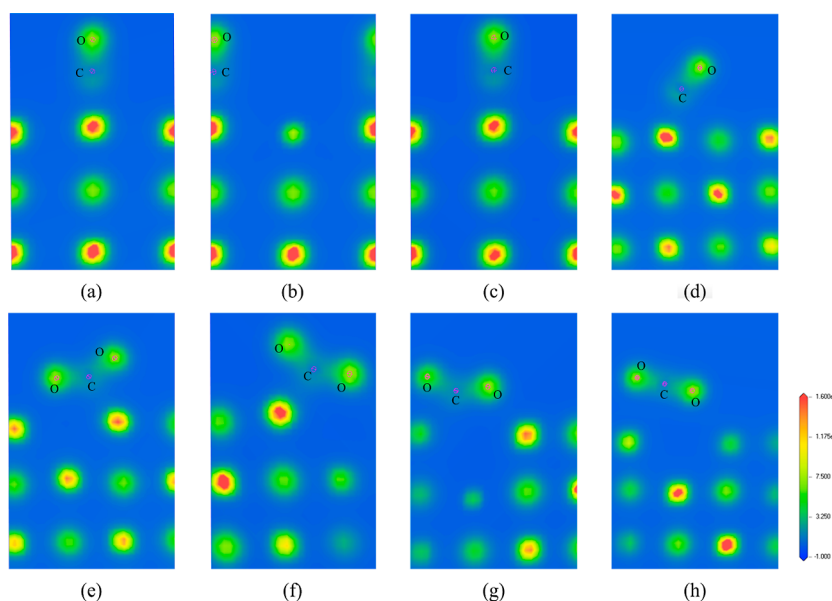
Figure 11. Electron density plots relative to CO adsorption sites on (a) pure NiO, (b) Li−NiO, (c) 2Li−NiO, and (d) 3Li−NiO; electron density plots of CO_2 on (e) pure NiO, (f) Li−NiO, (g) 2Li−NiO, and (h) 3Li−NiO surface.

of OCs surface.[6,52] The oxygen vacancy formation energies on the surface of Li-doped NiO were calculated to determine the influence of the dopant on the surface oxygen activity. The oxygen vacancy formation energies of NiO, Li−NiO, 2Li−NiO, and 3Li−NiO are exhibited, as shown in Figure 12. The
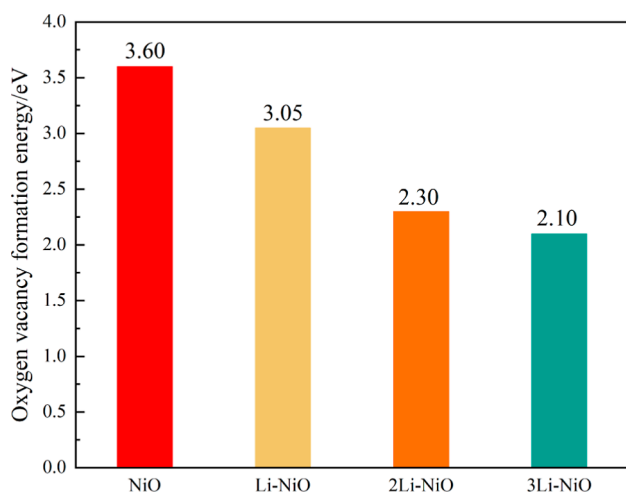

Figure 12. Oxygen vacancy formation energies of the NiO, Li−NiO, 2 Li−NiO, and 3Li−NiO surfaces.

oxygen vacancy formation energy for pure NiO is determined to be 3.60 eV. The oxygen vacancy formation energies for Li−NiO, 2Li−NiO, and 3Li−NiO are calculated to be 3.05, 2.30, and 2.10 eV, respectively. The oxygen vacancy formation energy of 3Li−NiO is approximately 1.50 eV lower than that of pure NiO. The results indicate that the oxygen vacancy formation energy in NiO diminishes as the concentration of Li doping escalates. The significant reduction suggests that Li doping has a pronounced effect on decreasing the oxygen vacancy formation energy. Consequently, the addition of Li dopant holds the potential to enhance the surface oxygen activity, which promotes the oxidation of CO on the OCs surface. The Li cation has a formal charge of +1 and can be

substituted for the Ni cation in NiO to generate an "electron deficit" in the doped region. The results indicate that this "electron deficit" leads to a weaker connection between the O atom and the doped NiO than the bond between the O atom and pure NiO.

4. CONCLUSIONS

The reaction mechanisms of Li-doped Ni-based OCs with various concentrations were comprehensively investigated at the atomic level in this study, employing the DFT computation. Three different Li doping concentrations of 4, 8, and 12% were considered. The adsorption energies of the doped surfaces are found to be higher compared with the undoped surfaces. The 3Li−NiO surface with a Li doping concentration of 12%, exhibits the highest affinity for CO adsorption. The findings suggest that Li doping enhances the surface adsorption of CO. The PDOS of free and CO structures after adsorption at the active site was studied. Following the adsorption reaction, the PDOS of CO shifts toward lower energy states. The results indicate that the adsorption of the CO molecule on the surface is stable. The CO oxidation processes on the pure and doped NiO surfaces were further investigated. The CO_2 formation energy barrier of pure NiO surfaces is 2.12 eV. The CO_2 formation energy barriers on NiO surfaces doped with concentrations of 4, 8, and 12% Li atoms are 0.73, 0.51, and 0.58 eV, respectively. By comparing each pathway, it is possible to deduce that CO molecules on the Li-doped surface are easily oxidized by surface oxygen to form CO_2 molecules due to their low energy barrier. The results show that adding Li as a dopant to NiO enhances reactivity. Additionally, oxygen vacancy formation energies were calculated for surfaces with different concentrations of Li-doped NiO. The oxygen vacancy formation energies at the NiO, Li−NiO, 2Li−NiO, and 3Li−NiO surfaces are 3.60, 3.05, 2.30, and 2.10 eV, respectively. The results indicate a gradual decline in the formation energy of oxygen vacancies as the concentration of Li doping increased. Considering the crucial role of reducing the energy barrier in enhancing the reactivity of oxygen carriers, a doping

concentration of 8% Li is identified as optimal for NiO in CLC. These findings provide valuable insights and theoretical recommendations for the screening, optimization, and design of Ni-based OCs.

AUTHOR INFORMATION

Corresponding Author

Minjun Wang − *School of Energy and Power, Jiangsu University of Science and Technology, Zhenjiang 212003, China;* orcid.org/0009-0005-1863-2780; Email: wmj403@just.edu.cn

Authors

Mengke Wang − *School of Energy and Power, Jiangsu University of Science and Technology, Zhenjiang 212003, China*

Ming Xia − *School of Energy and Power, Jiangsu University of Science and Technology, Zhenjiang 212003, China*

Bixiao Zhang − *School of Energy and Power, Jiangsu University of Science and Technology, Zhenjiang 212003, China*

Yidan Wei − *School of Energy and Power, Jiangsu University of Science and Technology, Zhenjiang 212003, China*

Complete contact information is available at:
https://pubs.acs.org/10.1021/acsomega.3c08321

Author Contributions

Data curation: Mengke Wang and Minjun Wang; Investigation: Mengke Wang, Minjun Wang, Ming Xia, Bixiao Zhang and Yidan Wei; Writing—original draft: Mengke Wang, Bixiao Zhang and Yidan Wei; Writing—review and editing: Minjun Wang, Mengke Wang and Ming Xia. All authors have read and agreed to the published version of the manuscript.

Notes

The authors declare no competing financial interest.

ACKNOWLEDGMENTS

REFERENCES

(1) Abuelgasim, S.; Wang, W. J.; Abdalazeez, A. A brief review for chemical looping combustion as a promising CO_2 capture technology: Fundamentals and progress. *Sci. Total Environ.* 2021, 764, 142892.

(2) Wang, M. J.; Zhang, S. X.; Xia, M.; Wang, M. K. A Theoretical Study of the Oxygen Release Mechanisms of a Cu-Based Oxygen Carrier during Chemical Looping with Oxygen Uncoupling. *Catalysts* 2022, 12 (3), 332.

(3) Yuan, Y.; Dong, X. Q.; Ricardez-Sandoval, L. A multi-scale simulation of syngas combustion reactions by Ni-based oxygen carriers for chemical looping combustion. *Appl. Surf. Sci.* 2020, 531, 147277.

(4) Adanez, J.; Abad, A.; Mendiara, T.; Gayan, P.; de Diego, L. F.; Garcia-Labiano, F. Chemical looping combustion of solid fuels. *Prog. Energy Combust. Sci.* 2018, 65, 6−66.

(5) Hossain, M. M.; de Lasa, H. I. Chemical-looping combustion (CLC) for inherent CO_2 separations-a review. *Chem. Eng. Sci.* 2008, 63 (18), 4433−4451.

(6) Li, Z. P.; Tang, H. J.; Sun, Z. K.; Chen, C.; Duan, L. B. Unraveling the Structure-Reactivity Relationship of $CuFe_2O_4$ Oxygen Carriers for Chemical Looping Combustion: A DFT Study. *Energy Fuels* 2023, 37 (14), 10521−10530.

(7) Ksepko, E.; Lysowski, R. Stable Mixed Fe-Mn Oxides Supported on ZrO_2 Oxygen Carriers for Practical Utilization in CLC Processes. *Catalysts* 2021, 11 (9), 1047.

(8) Lin, S.; Gu, Z. H.; Zhu, X.; Wei, Y. G.; Long, Y. H.; Yang, K.; He, F.; Wang, H.; Li, K. Z. Synergy of red mud oxygen carrier with MgO and NiO for enhanced chemical-looping combustion. *Energy* 2020, 197, 117202.

(9) Kate, R. S.; Khalate, S. A.; Deokate, R. J. Overview of nanostructured metal oxides and pure nickel oxide (NiO) electrodes for supercapacitors: A review. *J. Alloys Compd.* 2018, 734, 89−111.

(10) Ahmad, A.; Al Mamun, M. A.; Al-Mamun, M.; Huque, S.; Ismail, M. LFO Perovskites as Oxygen Carriers for Chemical Looping Oxygen Uncoupling (CLOU). *J. Therm. Anal. Calorim.* 2022, 147 (12), 6605−6613.

(11) Kuang, C.; Wang, S. Z.; Lv, S.; Cai, J. J.; Luo, M.; Zhao, J. Comparison of metallic oxide, natural ore and synthetic oxygen carrier in chemical looping combustion process. *Int. J. Hydrogen Energy* 2021, 46 (34), 18032−18041.

(12) Ksepko, E. Examining $SrCuO_2$ as an oxygen carrier for chemical looping combustion. *J. Therm. Anal. Calorim.* 2015, 122 (2), 621−633.

(13) Mishra, A.; Li, T. Y.; Li, F. X.; Santiso, E. E. Oxygen Vacancy Creation Energy in Mn-Containing Perovskites: An Effective Indicator for Chemical Looping with Oxygen Uncoupling. *Chem. Mater.* 2019, 31 (3), 689−698.

(14) Adanez, J.; Abad, A. Chemical-looping combustion: Status and research needs. *Proc. Combust. Inst.* 2019, 37 (4), 4303−4317.

(15) Siriwardane, R. V.; Ksepko, E.; Tian, H. J.; Poston, J.; Simonyi, T.; Sciazko, M. Interaction of iron-copper mixed metal oxide oxygen carriers with simulated synthesis gas derived from steam gasification of coal. *Appl. Energy* 2013, 107, 111−123.

(16) De Vos, Y.; Jacobs, M.; Van der Voort, P.; Van Driessche, I.; Snijkers, F.; Verberckmoes, A. Development of Stable Oxygen Carrier Materials for Chemical Looping Processes-A Review. *Catalysts* 2020, 10 (8), 926.

(17) Ksepko, E.; Lysowski, R. Reactivity Study of Bimetallic Fe-Mn Oxides with Addition of TiO_2 for Chemical Looping Combustion Purposes. *Catalysts* 2021, 11 (12), 1437.

(18) Bayham, S. C.; Tong, A.; Kathe, M.; Fan, L. S. Chemical looping technology for energy and chemical production. *Wiley Interdiscip. Rev. Energy. Environ.* 2016, 5 (2), 216−241.

(19) Luo, S. W.; Zeng, L.; Fan, L. S. Chemical Looping Technology: Oxygen Carrier Characteristics. In *Annual Review of Chemical and Biomolecular Engineering, Vol 6*; Prausnitz, J. M., Ed.; Annual Reviews, 2015; Vol. 6, pp 53−75.

(20) Sun, Z. K.; Lu, D. Y.; Ridha, F. N.; Hughes, R. W.; Filippou, D. Enhanced performance of ilmenite modified by CeO_2, ZrO_2, NiO, and Mn_2O_3 as oxygen carriers in chemical looping combustion. *Appl. Energy* 2017, 195, 303−315.

(21) Blas, L.; Dorge, S.; Michelin, L.; Dutournie, P.; Lambert, A.; Chiche, D.; Bertholin, S. Influence of the regeneration conditions on the performances and the microstructure modifications of NiO/$NiAl_2O_4$ for chemical looping combustion. *Fuel* 2015, 153, 284−293.

(22) Cheng, X. M.; Gu, Z. H.; Li, F. S.; Zhu, X.; Wei, Y. G.; Zheng, M.; Tian, D.; Wang, H.; Li, K. Z. Enhanced resistance to carbon deposition in chemical-looping combustion of methane: Synergistic effect of different oxygen carriers via sequence filling. *Chem. Eng. J.* 2021, 421, 129776.

(23) Feng, Y. C.; Wang, N. N.; Guo, X. Density functional theory study on improved reactivity of alkali-doped Fe_2O_3 oxygen carriers for chemical looping hydrogen production. *Fuel* 2019, 236, 1057−1064.

(24) Wang, M. J.; Liu, J.; Hu, J. B.; Liu, F. O_2-CO_2 Mixed Gas Production Using a Zr-Doped Cu-Based Oxygen Carrier. *Ind. Eng. Chem. Res.* 2015, 54 (40), 9805−9812.

(25) Li, Y.; Liu, J.; Liu, F.; Yang, Y. J. Computational design and experimental validation of transition-metal doped CuFe2O4 as oxygen carriers in chemical-looping combustion. *Fuel* 2022, 330, 125584.

(26) Chen, S. B.; Xiang, W. G.; Chen, S. Y. Modification of Metal (Fe, Al) Doping on Reaction Properties of a NiO Oxygen Carrier with CO during Chemical Looping Combustion. *ACS Omega* **2022**, 7 (5), 4381−4388.

(27) Zhang, J. P.; Zhang, H.; Yuan, N. N.; Meng, L. L.; Geng, C.; Bai, H. C. Insights into reactive behaviors and mechanisms of nickel-based oxygen carriers doped by Fe/Co during chemical looping combustion from multiple-scale molecular modeling combined with experiments. *Fuel Process. Technol.* **2022**, 229, 107181.

(28) Yuan, N. N.; Bai, H. C.; An, M.; Zhang, J. P.; Hu, X. D.; Guo, Q. J. Modulation of Fe-based oxygen carriers by low concentration doping of Cu in chemical looping process: Reactivity and mechanism based on experiments combined with DFT calculations. *Powder Technol.* **2021**, 388, 474−484.

(29) Liu, L.; Zachariah, M. R. Enhanced Performance of Alkali Metal Doped Fe_2O_3 and Fe_2O_3/Al_2O_3 Composites As Oxygen Carrier Material in Chemical Looping Combustion. *Energy Fuels* **2013**, 27 (8), 4977−4983.

(30) Xu, X. L.; Li, L.; Huang, J.; Jin, H.; Fang, X. Z.; Liu, W. M.; Zhang, N.; Wang, H. M.; Wang, X. Engineering Ni^{3+} Cations in NiO Lattice at the Atomic Level by Li^+ Doping: The Roles of Ni^{3+} and Oxygen Species for CO Oxidation. *ACS Catal.* **2018**, 8 (9), 8033−8045.

(31) Xu, X.; et al. Tuning Ni^{3+} quantity of NiO via doping of cations with varied valence states: The key role of Ni^{3+} on the reactivity. *Appl. Surf. Sci.* **2021**, 550, 149316.

(32) Cheng, Z.; Baser, D. S.; Nadgouda, S. G.; Qin, L.; Fan, J. A.; Fan, L. S. C_2 Selectivity Enhancement in Chemical Looping Oxidative Coupling of Methane over a Mg-Mn Composite Oxygen Carrier by Li-Doping-Induced Oxygen Vacancies. *ACS Energy Lett.* **2018**, 3 (7), 1730−1736.

(33) Segall, M. D.; Lindan, P. J. D.; Probert, M. J.; Pickard, C. J.; Hasnip, P.; Clark, S. J. MCPayne, First-principles simulation: ideas, illustrations and the CASTEP code. *J. Phys. Condens. Matter* **2002**, 14, 2717.

(34) White, J. A.; Bird, D. M. Implementation of gradient-corrected exchange-correlation potentials in Car-Parrinello total-energy calculations. *Phys. Rev. B Condens. Matter* **1994**, 50 (7), 4954−4957.

(35) Perdew, J. P.; Chevary, J. A.; Vosko, S. H.; Jackson, K. A.; Pederson, M. R.; Singh, D. J.; Fiolhais, C. Atoms, molecules, solids, and surfaces: Applications of the generalized gradient approximation for exchange and correlation. *Phys. Rev. B Condens. Matter* **1992**, 46 (11), 6671−6687.

(36) Vanderbilt, D. Soft self-consistent pseudopotentials in a generalized eigenvalue formalism. *Phys. Rev. B Condens. Matter* **1990**, 41 (11), 7892−7895.

(37) Castell, M. R.; Wincott, P. L.; Condon, N. G.; Muggelberg, C.; Thornton, G.; Dudarev, S. L.; Sutton, A. P.; Briggs, G. A. D. Atomic-resolution STM of a system with strongly correlated electrons: NiO(001) surface structure and defect sites. *Phys. Rev. B* **1997**, 55, 7859−7863.

(38) Zhang, J. P.; Gao, H. F.; Yuan, N. N.; Wang, Q.; Wu, Y. H.; Sun, Y. L.; Bai, H. C. Insights into the intrinsic interaction between series of C1 molecules and surface of NiO oxygen carriers involved in chemical looping processes. *Chin. J. Chem. Eng.* **2020**, 28 (11), 2771−2777.

(39) Yan, M.; Chen, S. P.; Mitchell, T. E.; Gay, D. H.; Vyas, S.; Grimes, R. W. Atomistic studies of energies and structures of (hk0) surfaces in NiO. *Philos. Mag. A* **1995**, 72 (1), 121−138.

(40) Yuan, Y.; Dong, X. Q.; Ricardez-Sandoval, L. A multi-scale model for syngas combustion on NiO oxygen carrier for chemical looping combustion: The role of nearest neighbors. *Fuel Process. Technol.* **2022**, 229, 107172.

(41) Cinquini, F.; Giordano, L.; Pacchioni, G. Adsorption of transition metal atoms on the NiO(100) surface and on NiO/Ag(100) thin films. *Theor. Chem. Acc.* **2008**, 120 (4−6), 575−582.

(42) Peng, G. W.; Merte, L. R.; Knudsen, J.; Vang, R. T.; Lægsgaard, E.; Besenbacher, F.; Mavrikakis, M. On the Mechanism of Low-Temperature CO Oxidation on Ni(111) and NiO(111) Surfaces. *J. Phys. Chem. C* **2010**, 114 (49), 21579−21584.

(43) Sawatzky, G. A.; Allen, J. W. Magnitude and origin of the band gap in NiO. *Phys. Rev. Lett.* **1984**, 53 (24), 2339−2342.

(44) Feng, Y. C.; Guo, X. Study of reaction mechanism of methane conversion over Ni-based oxygen carrier in chemical looping reforming. *Fuel* **2017**, 210, 866−872.

(45) Yu, N.; Zhang, W. B.; Wang, N.; Wang, Y. F.; Tang, B. Y. Water adsorption on a NiO(100) surface: A GGA+U study. *J. Phys. Chem. C* **2008**, 112 (2), 452−457.

(46) Feng, Y. C.; Cai, X.; Guo, X.; Zheng, C. G. Influence mechanism of H_2S on the reactivity of Ni-based oxygen carriers for chemical-looping combustion. *Chem. Eng. J.* **2016**, 295, 461−467.

(47) Sorescu, D. C. Adsorption and activation of CO coadsorbed with K on Fe(100) surface: A plane-wave DFT study. *Surf. Sci.* **2011**, 605 (3−4), 401−414.

(48) Zheng, T.; Li, M. J.; Mei, D. F.; Ma, J. J.; Wang, B. W.; Xu, Z. W. Effect of H_2S presence on chemical looping reforming (CLR) of biogas with a firebrick supported NiO oxygen carrier. *Fuel Process. Technol.* **2022**, 226, 107088.

(49) Srivastava, N.; Srivastava, P. C. Realizing NiO nanocrystals from a simple chemical method. *Bull. Mater. Sci.* **2010**, 33 (6), 653−656.

(50) Apell, S. P.; Sabin, J. R.; Oddershede, J. Molecular shape and the Bragg rule. *Phys. Rev. A* **2002**, 66 (3), 034701.

(51) Cai, X.; Wang, X. H.; Guo, X.; Zheng, C. G. Mechanism study of reaction between CO and NiO(001) surface during chemical-looping combustion: Role of oxygen. *Chem. Eng. J.* **2014**, 244, 464−472.

(52) Ganduglia-Pirovano, M. V.; Popa, C.; Sauer, J.; Abbott, H.; Uhl, A.; Baron, M.; Stacchiola, D.; Bondarchuk, O.; Shaikhutdinov, S.; Freund, H. J. Role of ceria in oxidative dehydrogenation on supported vanadia catalysts. *J. Am. Chem. Soc.* **2010**, 132 (7), 2345−2349.